



ELSEVIER

Available online at www.sciencedirect.com

SCIENCE @ DIRECT®

Journal of Environmental Radioactivity 75 (2004) 59–82

JOURNAL OF
ENVIRONMENTAL
RADIOACTIVITY

www.elsevier.com/locate/jenvrad

Simulation of the dispersion of nuclear contamination using an adaptive Eulerian grid model

I. Lagzi^{a,*}, D. Kármán^a, T. Turányi^a, A.S. Tomlin^b,
L. Haszpra^c

^a Department of Physical Chemistry, Eötvös University, H-1518 Budapest, P.O. Box 32, Hungary

^b Department of Fuel and Energy, The University of Leeds, Leeds, LS2 9JT, UK

^c Institute for Atmospheric Physics, Hungarian Meteorological Service, H-1675 Budapest, P.O. Box 39, Hungary

Received 11 February 2003; received in revised form 1 October 2003; accepted 7 November 2003

Abstract

Application of an Eulerian model using layered adaptive unstructured grids coupled to a meso-scale meteorological model is presented for modelling the dispersion of nuclear contamination following the accidental release from a single but strong source to the atmosphere. The model automatically places a finer resolution grid, adaptively in time, in regions where high spatial numerical error is expected. The high-resolution grid region follows the movement of the contaminated air over time. Using this method, grid resolutions of the order of 6 km can be achieved in a computationally effective way. The concept is illustrated by the simulation of hypothetical nuclear accidents at the Paks NPP, in Central Hungary. The paper demonstrates that the adaptive model can achieve accuracy comparable to that of a high-resolution Eulerian model using significantly less grid points and computer simulation time.

© 2004 Elsevier Ltd. All rights reserved.

Keywords: Dispersion of nuclear contamination; Eulerian model; Adaptive grid; Accidental release

* Corresponding author. Tel.: +36-12090555; fax: +36-12090602.

E-mail address: lagzi@vuk.chem.elte.hu (I. Lagzi).

1. Introduction

Modelling the accidental release of radioactive or chemically toxic substances requires the study of long-range transport from a single concentrated emission source. The path of the resulting plume should be predicted, along with its time of arrival to populated locations, and the possible levels of exposure to pollutants or deposition over a potentially large area. The simulations must have a high degree of accuracy and yet must be achieved faster than real time to be of use in decision support. Integrated models such as RODOS are now attempting to incorporate predictive models with decision making strategies, and in fact, model predictions are often the key input to decisions on emergency response and environmental management (Galmarini et al., 2001; Whicker et al., 1999; Baklanov et al., 2002). To carry out successful and cost effective strategies requires a very accurate prediction of the location of the contaminant plume and concentrations. Underestimating the maximum dosage may have serious health consequences, and conversely, applying remediation measures in regions where significant dosage will not be received would waste valuable resources and may have significant social implications if evacuation is required. The consequences of predicting the presence of a pollutant where none exists, or the absence of a pollutant where it is actually present, therefore make high demands on model predictions.

Following the Chernobyl accident most countries in Europe developed national nuclear dispersion or accidental release models linked to weather prediction models of varying types and resolutions. Galmarini et al. (2001) list 22 programs of this type using differing modelling strategies, and also present a method for statistically evaluating the predictions from a large number of codes, which may give different solutions. The performance of a number of these models was evaluated against the ETEX European tracer experiments (Van Dop et al., 1998) with no overall modelling strategy emerging from this evaluation as being statistically better than another. A comparative discussion of the available model types will be given in the next section. The second ETEX experiment proved to be a challenge for all the codes, since they failed to predict the location of the tracer plume accurately. Clearly therefore, issues still remain as to what is an appropriate strategy for predicting the impact of an accidental release. Sensitivity tests from the ETEX comparisons showed significant impact of both input data (e.g. three dimensional wind-fields and boundary layer descriptions) and model structure, such as the choice of numerical solution method and model resolution on output predictions.

Models are not only used for predictive purposes such as exposure assessment, but are also often used to test our understanding of the underlying science that forms the foundation of the models. Improvements in our understanding are often tested by comparison of the models with measured data. If this is the case then one must be sure that changes made to input data to improve predictions are not compensating for errors that actually arise from the numerical solution of the problem. It follows that models used within the decision making and environmental management context must use not only the best available scientific knowledge and data, but also the best available numerical techniques. By this we mean techniques that

minimise the errors induced by the choice of numerical solution method rather than the structure of the physical model. Because of the historical development of environmental predictive models and the investment time required to implement new computational solution strategies, unfortunately the most appropriate numerical method is not always used. Therefore, the aim of this work is not to elaborate yet another numerical dispersion simulation code, but to present the practical application of improved numerical methods which may provide useful developments to some existing modelling strategies. The paper presents the use of adaptive Eulerian grid simulations to accidental release problems and it will be shown by comparison with some current numerical computational methods that improvements in accuracy can be made without significant extra computational expense.

The paper is structured as follows. Section 1.1 provides an introductory discussion of existing model types for the prediction of the dispersion from accidental releases. Section 1.2 discusses the importance of the structure of the underlying meteorological model. Section 2 describes the physical model used for the present simulations and the adaptive numerical methods used to solve the resulting equations. Section 3 presents the use of the model for the prediction of hypothetical accidents from the Paks NPP in Central Hungary and includes a discussion of the comparison of the present method with more traditional modelling approaches. Section 4 presents some final conclusions from the work and its significance for the modelling of dispersion from accidental releases.

1.1. Discussion of existing model types

The Chernobyl release provided a large impetus for the development of accidental release models and several intercomparisons between different model types have since been made (Galmarini et al., 2001; Van Dop et al., 1998; Wendum, 1998). The predominant model types are Lagrangian and Eulerian. The former trace air masses, particles with assigned mass, or Gaussian shaped puffs of pollutants along trajectories determined by the wind-field structures. Lagrangian models have the advantage that they can afford to use high spatial resolution although they rely on the interpolation of meteorological data. Their potential disadvantages are that in some cases they neglect important physical processes and often experience problems when strongly diverging flows lead to uncertainties in long-range trajectories. One example of this is discussed by Baklanov et al. (2002) who modelled the potential transport of radionuclides across Europe and Scandinavia from a hypothetical accident in Northern Russia using an isentropic trajectory model. In their ‘winter’ case studies the isentropic trajectory model simulated much of the deposition when compared to a high-resolution meteorological/dispersion model. In some cases however, additional deposition was predicted by the dispersion model in locations not predicted by the isentropic trajectory model due to the splitting of atmospheric trajectories.

There are several types of Lagrangian trajectory models. One example of a Gaussian puff model is the DERMA model (Sørensen, 1998), which uses a multi-puff

diffusion parameterisation. A Gaussian profile is assumed for the puff in the horizontal direction with complete mixing in the vertical direction within the boundary layer and a Gaussian profile above it. The UK MET office NAME model (Bryall and Maryon, 1998) and the Norwegian SNAP model (Saltbones et al., 1998) use a Lagrangian particle formulation, which resolves the trajectories of a large number of particle releases with assigned masses. The NAME model is capable of following a 3D mean wind-field plus a turbulent component with a variety of turbulence parameterisations available ranging from simple eddy diffusion terms to complex random walk descriptions, although the turbulent parameterisations are based on measurements from a single location. Because it does not use a Gaussian puff formulation it can resolve varying wind-speeds and directions, skewed turbulence and varying stabilities. The disadvantage of this approach is its computational expense, since a large number of particles must be released when compared to the Gaussian puff approach.

Eulerian models use grid based methods and have the advantage that they may take into account fully 3D descriptions of the meteorological fields rather than single trajectories (Wendum, 1998; Langner et al., 1998). However, when used traditionally with fixed meshes, Eulerian models show difficulty in resolving steep gradients. This causes particular problems for resolving dispersion from a single point source, which will create very large gradients near the release. If a coarse Eulerian mesh is used then the release is immediately averaged into a large area, which smears out the steep gradients and creates a large amount of numerical diffusion. The result will be to underpredict the maximum concentrations within the near-field plume and to over estimate the plume width. Close to the source the problem could be addressed by nesting a finer resolution grid to better resolve steep gradients.

This need to resolve accurately both near and far field dispersion has been noted previously by for example Brandt et al. (1996) who used a combined approach of a Lagrangian meso-scale model coupled with a long range Eulerian transport model in the development of the DREAM model. The approach requires some kind of interpolation procedure between the two grids. A similar approach was also employed through the point source initialisation scheme in the Swedish Eulerian model MATCH (Langner et al., 1998). The MATCH model uses a Lagrangian particle model for the horizontal transport of the first 10 h after the point source release with vertical transport being described by an Eulerian framework during this time. Quite a large number of particles need to be released per hour to reduce errors in predicting the vertical transport, thus adding to the computational cost. These multi-scale modelling approaches showed significant improvements in predictions close to the release due to the higher resolution Lagrangian models. However, as with the nested Eulerian modelling approach, they still suffer from the drawback that the plume is averaged into the larger Eulerian grid as soon as it leaves the near source region. Brandt et al. (1996) argue that once the plume has left the near-source region the gradients will become sufficiently smooth as to lead to small errors due to numerical diffusion. This ignores however, the fact that steep gradients may persist at plume edges for large distances from the source due to

meso-scale processes. Previous studies have shown that high contamination levels or deposition can exist over small areas several hundred kilometres from the source (Baklanov et al., 2002).

Brandt et al. (1996) argue that long-range Eulerian models are not suitable for resolving single source releases alone and demonstrate this through the standard Molenkamp test of a rotating passive puff release in a circular wind-field. More recently, however, it has been shown (Ghorai et al., 2000; Lagzi et al., 2001, 2002; Tomlin et al., 2000) that adaptive Eulerian methods are very capable of resolving the advection of such single source releases since they can automatically refine the mesh in regions where steep gradients exist. Moreover, they can be more efficient than say nested models, since they refine only where high spatial numerical errors are found and not in regions where grid refinement is not necessary for solution accuracy. This means that for the same computational run-time they may allow higher resolution of the grid in important areas. Eulerian models also provide an automatic framework for the description of mixing processes and non-linear chemical reaction terms. This paper will therefore show that adaptive grid methods provide a consistent approach to coupling near-field and long-range simulations for single source accidental releases.

1.2. Resolution of input meteorological data

It is clear that one of the most crucial inputs to any dispersion model for point source releases is the underlying meteorological data such as wind-field and boundary layer descriptions. The importance of the horizontal resolution of meteorological data has been demonstrated by many of the simulations of the first ETEX experiment. The ETEX experiment was an international tracer campaign during which a passive tracer was tracked across Europe over several days from its release in France by monitoring at a large number of meteorological stations (Van Dop et al., 1998). Many numerical simulations were carried out which demonstrated the need for meso-scale weather modelling. Nasstrom and Pace (1998) for example showed that events resolved by a meteorological model of 45 km but not at 225 km resolution had a significant impact on even long-range dispersion of the ETEX plume. Sørensen (1998) showed that the double structure of the first ETEX plume was picked up by their model when using meso-scale weather predictions but not when using coarser resolution ECMWF data. The difference was attributed to a meso-scale horizontal anti-cyclonic eddy that was not resolved within the ECMWF data. The importance of resolving the vertical structure of wind-speeds and directions was demonstrated by the second ETEX experiment where evidence of decoupling of an upper cloud of pollution from the boundary layer plume was observed (Bryall and Maryon, 1998). In this case significant concentrations were measured behind the path of the plume predicted by most of the models tested. This behaviour has been attributed to the vertical lofting of the plume by the passage of a front, followed by the transport of the pollution cloud in upper

levels of the atmosphere at a lower wind-speed that in the boundary layer or even perhaps in a different wind-direction. The MET Office NAME model in this case showed a significant amount of mass above the boundary layer for the second ETEX experiment in contrast to the first one where particles were well distributed throughout the boundary layer.

Previous simulations point to several important issues relating to the development of an accidental release model. Firstly, a meso-scale meteorological model must be used in order to capture small spatial scale effects such as frontal passages and small scale horizontal eddies. Secondly, the dispersion model used must be capable of representing, in some way, the possible vertical variations in wind speed and direction, rather than using a single boundary layer description with varying mixing layer height but a single wind-field. Thirdly, the dispersion model must be capable of resolving potentially steep concentration gradients that may be caused by either the single source release or features that may arise due to meso-scale meteorological events. This paper will therefore discuss the practical application of an adaptive Eulerian dispersion model when coupled to data from a high-resolution meso-scale meteorological model.

2. Model description and numerical methods

2.1. Dispersion simulation using unstructured adaptive grid algorithms

The model used in the current work was developed via a co-operation between the University of Leeds, the Eötvös University (Budapest) and the Hungarian Meteorological Service and describes the spread of reactive air pollutants within an unstructured triangular based grid representing layers of the troposphere over the Central European region. The model has been developed within a flexible framework and can therefore simulate both single source accidental releases and photochemical air pollution, where the pollution sources are both area and point sources and the chemical transformations are highly non-linear. A slightly modified version of the model is used here to demonstrate its capacity simulating nuclear dispersion calculations.

In the model, the horizontal dispersion of radionuclides is described within an unstructured triangular Eulerian grid framework. The vertical mixing of radionuclides is approximated by a parameterised description of mixing between four layers representing the surface, mixing, reservoir layers and the free troposphere (upper) layer. The horizontal grid is adaptive, i.e. continuously changes in space and time to minimise the numerical errors. The transformation of radionuclides is described within each grid cell by the equations of nuclear decay. Transient refinement and de-refinement is then further invoked as necessary throughout the model run according to spatial errors and chosen refinement criteria. A basic model description will be given below.

2.2. Numerical method

The atmospheric transport diffusion equation in two space dimensions is given by

$$\frac{\partial c_i}{\partial t} = -\frac{\partial(uc_i)}{\partial x} - \frac{\partial(vc_i)}{\partial y} + \frac{\partial}{\partial x} \left(K_x \frac{\partial c_i}{\partial y} \right) + \frac{\partial}{\partial y} \left(K_y \frac{\partial c_i}{\partial x} \right) + R_i + E_i - (k_{wi} + d_{di})c_i, \quad (1)$$

where c_i is the concentration of radionuclide i ; u , v , are the components of horizontal wind velocity, K_x and K_y are turbulent diffusivity coefficients and k_{wi} and k_{di} are the wet and dry deposition coefficients, respectively. E_i describes the emission sources for the i th radionuclide and R_i is the nuclear build up or decay term. For n radionuclides an n -dimensional set of partial differential equations (PDEs) is formed describing the rates of change of radionuclides over time and space, where the equations are coupled through nuclear decay terms.

The basis of the numerical method is the spatial discretisation of the PDEs derived from the atmospheric transport-diffusion equation on unstructured triangular meshes using the software SPRINT2D (Berzins et al., 1992). For advection dominated problems it is important to choose a discretisation scheme that preserves the physical range of the solution and therefore the model uses the flux limited, cell centred finite volume scheme (Berzins and Ware, 1994, 1995; Ware and Berzins, 1995). This approach, known as the ‘method of lines’, reduces the set of PDEs in three independent variables to a system of ordinary differential equations (ODEs) in one independent variable, time. This is achieved by the integration of the atmospheric diffusion equation over each finite volume, the use of the divergence theorem and the evaluation of the line integral along the boundary of each volume using the midpoint quadrature rule. The system of ODEs can then be solved as an initial value problem, and a variety of powerful software tools exist for this purpose (Berzins et al., 1989). A more in-depth discussion of the methods can be found in references (Berzins et al., 1989, 1992; Berzins and Ware, 1994, 1995; Berzins, 1994; Tomlin et al., 1997; Hart et al., 1998; Hart, 1999).

The model domain is represented by an unstructured mesh of triangular elements surrounding each grid point, thus forming a small volume over which the solution is averaged. The model therefore falls into the category of Eulerian models described above, although it is not described by the standard Cartesian mesh approach. The use of adaptivity however, allows the model to overcome the usual problems of the Eulerian approach, since a fine mesh can be used where needed leading to averaging over small volumes. The term ‘unstructured’ represents the fact that each node in the mesh may be surrounded by any number of triangles, whereas in a structured mesh such as a Cartesian mesh, the number of surrounding grid points would be fixed. The use of an unstructured mesh easily enables the adequate resolution of complex solution structures that may be found following point source releases and which may not fall naturally into Cartesian geometrical descriptions. For example, following release, the plume from a point source may be stretched and folded in space due to advection and turbulent mixing. The unstructured triangular mesh then provides an efficient way of adapting around this

complex geometry. The initial unstructured triangular meshes used in the model are created from a geometry description using the Geompack mesh generator (Joe and Simpson, 1991).

The complex nature of atmospheric dispersion problems makes the pre-specification of grid densities very difficult, particularly for forecasting codes where the wind-field is not known in advance. Many complex processes can take place far from the source due to advection, mixing, chemical reactions and deposition, affecting the geometry of the plume and spatial concentration profiles. To this end the model presented here utilises adaptive gridding techniques, which quantitatively evaluate the accuracy of the numerical solution in space and time and then automatically refine or de-refine the mesh where necessary. As described above, the accuracy of Eulerian models tends to become degraded in regions where the concentration of the pollutant changes steeply in space. The use of transient adaptivity allows us to overcome this problem. It is achieved by using a tree-like data structure with a method of refinement based on the regular subdivision of triangles (local h-refinement). Here an original triangle is split into four similar triangles as shown in Fig. 1 by connecting the midpoints of the edges. Hanging or unconnected nodes are removed by joining them with nearby vertices. This finer grid may be later coalesced into the parent triangle to coarsen the mesh if the solution accuracy does not require refinement—for example when the plume has passed or concentration gradients in space are reduced. The use of unstructured meshes allows the model to go from very fine resolution to coarse resolution within small spatial regions.

Once a method of refinement has been implemented, a suitable criterion for the application of transient adaptivity must be chosen. The technique used here is based on the calculation of spatial error estimates, allowing a certain amount of automation to be applied to the refinement process. This is achieved by first calculating some measure of numerical error in each species over each triangle. A reliable method for determining the numerical error is to examine the difference between the solution gained using a high accuracy and a low accuracy numerical method. Over regions of high spatial gradient in concentrations the difference between high and low order solutions will be greater than in regions of relatively smooth solution, and refinement generally takes place in these regions, such as at

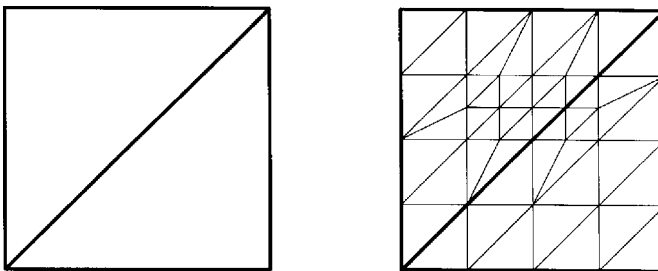


Fig. 1. Example of local h-refinement.

plume edges. A refinement indicator for the j th triangle is defined by an average scaled error measured over all $npde$ PDEs using absolute ($atol$) and relative ($rtol$) tolerances supplied by the user:

$$serr_j = \sum_{i=1}^{npde} \frac{e_{i,j}(t)}{\frac{atol_i}{A_j} + rtol_i \times c_{i,j}}, \quad (2)$$

where $c_{i,j}$ is the computed concentration of species i in triangle j . $e_{i,j}(t)$ is the difference between the solution using a first order method and that using a second order method. A_j is the area of triangle j . This allows the user to weight the refinement towards a chosen species error and also to control the extent of refinement by providing tighter or looser tolerances. The use of absolute as well as relative tolerances allows the user to define a species concentration below which high relative accuracy is not required. For the current example the choice of this tolerance may be driven by a minimum concentration of concern from a health point of view for example. An integer refinement level indicator is calculated from the scaled error above to give the number of times the triangle should be refined or de-refined. The choice of tolerances will therefore reflect, to a certain extent, a balance between desired accuracy and available computational resources, since tighter tolerances usually lead to a higher number of grid cells. It is also possible within the code for the user to control the maximum number of levels of adaptivity, thus limiting the minimum grid size in regions of very steep gradients i.e. close to the point source. Since the error is applied at the end of time-step it is too late to make refinement decisions. Methods are therefore used for the prediction of the growth of the spatial error using quadratic interpolants. The spatial error can therefore be used to predict within which regions the grid should be refined or coarsened for the next time-step in order to give good spatial accuracy with the minimum computational resource.

The application of adaptive rectangular meshes would be also possible, but would be less effective in terms of the number of nodes required in order to achieve high levels of adaptivity. Although the data structures resulting from an unstructured mesh are somewhat more complicated than those for a regular Cartesian mesh, problems with hanging nodes at boundaries between refinement regions are avoided. The use of a flexible discretisation stencil also allows for an arbitrary degree of refinement, which is more difficult to achieve on structured meshes.

2.3. Physical model description

2.3.1. Model domain

The model domain covers Central Europe including Hungary with a domain size of 1550×1500 km. The model describes the domain using a Cartesian coordinate system through the stereographic polar projection of the curved surface onto a flat plane. Global coordinates are transformed by projecting the surface of the Earth, from the opposite pole onto a flat plane located at the North Pole that is perpendicular to the Earth's axis. Due to the orientation of the projection plane this

transformation places the Cartesian origin at the North Pole. The model includes four vertical atmospheric layers: a surface layer, a mixing layer, a reservoir layer and the free troposphere (upper) layer. The surface layer extends from ground level to 50 m altitude. Above the surface layer is the mixing layer whose height is determined for 0.00 and 12.00 UTC values by radiosonde measurements in Budapest. The night time values are assumed to be identical to the midnight value while the height between 6.30 and 15.00 were linearly interpolated between the night and the highest daytime values. The reservoir layer, if it exists, extends from the top of the mixing layer to an altitude of 1000 m. Different wind-fields are represented for each layer and vertical mixing and deposition are parameterised according to the vertical stratification presented by van Loon (1996).

2.3.2. Meteorological data

The local wind speed and direction was considered as a function of space and time. These data were obtained from the meso-scale meteorological model ALADIN (Horányi et al., 1996), which provides data with a time resolution of 6 h and a spatial resolution of $0.10 \times 0.15^\circ$. The ALADIN model is a hydrostatic, spectral limited area model using 24 vertical layers where initial and boundary conditions are determined from larger scale ECMWF data. The model domain for ALADIN covers the Central European region from latitude 43.1° to 52.0° and longitude 10.35° to 25.1° . The data from ALADIN were interpolated using mass conservative methods to obtain data relevant to a given space and time point on the adaptive model grid. The surface temperature and cloud coverage, relative humidity and wind-field for each layer were determined from the ALADIN database. The eddy diffusivity coefficients for the x and y directions were set at $50 \text{ m}^2 \text{ s}^{-1}$ for all species.

2.3.3. Dry deposition and vertical mixing

The species exchange between the layers (i.e. the vertical transport) is modelled in two ways. Exchange between the mixing and the surface layers due to turbulent diffusion was described by ODEs. At the top of the mixing layer fumigation occurs, which is also described by ODEs. This way, species exchange takes place between the mixing layer and the reservoir layer or the upper layer if the reservoir layer does not exist. Dry deposition and the exchange between the mixing layer and the surface layer was described by the following set of ODEs:

$$\frac{d(c_m H_m)}{dt} = -\beta v_g(H_s) c_m - \frac{1}{r_a(H_s)} \left(c_m - \frac{v_g(s)}{v_g(H_s)} c_s \right), \quad (3)$$

$$\frac{d(c_s H_s)}{dt} = -v_g(s) c_s - \frac{dc_m H_m}{dt}, \quad (4)$$

where

$$\beta = \frac{H_m}{H_m + \frac{v_g(H_s)}{v_g(s)} H_s}. \quad (5)$$

H_m and H_s are the depth of the mixing and surface layers, respectively and $s = 0.5H_s$. c_m and c_s are the concentrations in the mixing and surface layers and $v_g(z)$ is the deposition velocity at height z . r_a is the aerodynamic resistance. The parameterisation of dry deposition was based on the resistance method

$$v_g(z) = \frac{1}{r_c + r_s + r_a}, \tag{6}$$

where r_c is the surface resistance and r_s is the boundary layer resistance. Parameter $r_s = 2.6/\kappa u_*$, where κ is the von Karman constant and u_* is the friction velocity. Parameter r_c was set to 500 s m^{-1} for ^{131}I and ^{131}Xe (Verver and De Leeuw, 1992). The aerodynamic resistance was calculated according to

$$r_a = \frac{0.74}{\kappa u_* \left(\log \frac{z}{z_o} + \chi(z_o) - \chi(z) \right)}, \tag{7}$$

where

$$\begin{aligned} \chi(z) &= -6.4 \frac{z}{L}, \quad \text{if } L > 0 \\ \chi(z) &= 2 \ln \left(\sqrt{1 - 9 \frac{z}{L}} + 1 \right), \quad \text{if } L < 0. \end{aligned} \tag{8}$$

Parameter z_o is the roughness length and is taken to be 0.25 m representing medium size vegetation as typically found in an agricultural region. L is the Monin-Obukhov length, which was calculated according to the following method (COST Action 710, 1998):

1. At night ($R_g = 0$, where R_g is the global radiation)

$$T_* = \min(T_{*1}, T_{*2}) \tag{9}$$

$$T_{*1} = 0.09(1 - 0.5N^2), \quad T_{*2} = \frac{TC_{dn}V}{4\beta_M s g}, \tag{10}$$

where N is the cloud coverage, which varied between 0 and 1, g is the gravitational constant, T is the surface layer temperature and T_* represents the dynamic temperature. $\beta_M = 4.7$ and

$$C_{dn} = \frac{\kappa}{\ln(z) - \ln(z_o)}, \quad V = \sqrt{u^2 + v^2}. \tag{11}$$

$$u_* = \left(\frac{C_{dn}V}{2} (1 + (1 - \text{corr}^2))^{1/2} \right), \quad \text{if } \text{corr} \leq 1$$

$$u_* = \sqrt{\hat{L} \frac{T_*}{T} g \kappa}, \quad \text{if } \text{corr} > 1, \tag{12}$$

where $\hat{L} = 5$ m and

$$\text{corr} = \frac{2u_o}{C_{\text{dn}}^{1/2} V}, \quad u_o = \left(\frac{\beta_{\text{M}} s g T_*}{T} \right)^{1/2}. \quad (13)$$

2. During the daytime ($R_g > 0$)

$$u_* = \frac{\kappa u}{\ln(s) - \ln(z_o)}, \quad \text{if } V \geq 0.5 \text{ ms}^{-1}$$

$$u_* = 0.05 \text{ ms}^{-1}, \quad \text{if } V < 0.5 \text{ ms}^{-1} \quad (14)$$

$$T_* = -\frac{q}{\rho c_p u_*}, \quad (15)$$

where $\rho = 1.2754 \text{ kg m}^{-3}$, the density of air, $c_p = 1.005 \text{ J kg}^{-1} \text{ K}^{-1}$, the specific heat. The sensible heat flux q was calculated from the global radiation.

The Monin–Obukhov length is calculated from the following equation:

$$L = \frac{T u_*^2}{g \kappa T_*}. \quad (16)$$

Fumigation describes the process, which occurs as the height of the mixing layer changes. Species exchange takes place between the mixing layer and the reservoir layer (if it exists) and the upper layer if not. This process is modelled by the equation

$$\frac{d(H_m c_m)}{dt} = \frac{dH_m}{dt} c_{r,u}, \quad (17)$$

where $c_{r,u}$ is the concentration in the reservoir or upper layer.

2.3.4. Wet deposition

Wet deposition was parameterised using a simple scheme to calculate the scavenging coefficient k_w based on the relative humidity

$$k_w = 0, \quad \text{if } RH < RH_t$$

$$k_w = 3.5 \times 10^{-5} \left(\frac{RH - RH_t}{RH_s - RH_t} \right), \quad \text{if } RH \geq RH_t, \quad (18)$$

where RH is the relative humidity, RH_t (=80%) is the threshold value of the relative humidity where condensation is assumed to occur and RH_s (=100%) is the saturation value (Pudykiewicz, 1989, 1991; Clark and Smith, 1988).

3. Results showing the importance of adaptive gridding

The features of the model are illustrated by the simulation of a hypothetical nuclear accident on 2 August 1998, at time 0.00 in the Paks nuclear power plant. The release of 2.985 kg ^{131}I isotope is assumed at a height of 10 m for 12 h. This

isotope decays to the stable ^{131}Xe with a half-life of 6.948×10^5 s. In the current simulations, only the radioactive decay of ^{131}I was calculated and the change of activity of this isotope was simulated. The model is capable of the simultaneous simulation of the spread of several hundred isotopes, taking into account all radioactive decays.

Fig. 2a shows the initial grid for the adaptive and coarse grid calculations. The typical length of a triangle edge is 106 km and around the Paks NPP a somewhat finer resolution initial grid was used. The figure shows that the modelled area includes Hungary and covers the neighbouring countries within about 600 km from the border to all directions. Wind-field maps corresponding to this period indicated that the wind at all heights from the surface to 3000 m blew from south-east in the first 36 h. After this, the wind direction changed to northwest in the Czech Republic and Poland, but was almost unchanged in the other areas. The application of adaptive gridding methods was compared to the application of fixed grids for the hypothetical release described above. Three different fixed grid schemes were tested:

1. the initial grid (shown in Fig. 2a) was not refined during the calculations;
2. a high resolution (triangle edge length 6.6 km) nested grid was placed around the source within a $250 \text{ km} \times 250 \text{ km}$ area as shown in Fig. 2b;
3. a high resolution (triangle edge length 6.6 km) fixed grid was used within the whole area.

Fig. 3e–h show the simulated surface layer activity of isotope ^{131}I using adaptive gridding. A continuous release was assumed in the first 12 h and therefore there is a continuous plume after 12 h (Fig. 3e). After 12 h, the cloud is separated from the source and travels towards the northwest (t_0+24 h, Fig. 3f). After 36 h (Figs. 3g, h) it starts to drift backwards towards the southeast. Fig. 3a–d show that the region of increased grid resolution continuously follows the path of the contaminated air. The typical grid size in the non-contaminated area remained at *ca* 106 km, but in the highly contaminated area it was automatically reduced to 6.6 km (the minimum allowed length at the simulation) by the transient adaptation routine, allowing better spatial resolution in critical areas.

Figs. 4–7 compare the simulation results using the three fixed grid schemes at simulation times 12, 24, 36, and 48 h after the accident. The fine grid calculation has the lowest numerical error and therefore these results are the basis of comparison for the other mesh strategies. The coarse grid calculations show high numerical diffusion at all times. The result is that the initial plume is smeared over a much wider area than in the fine grid simulation as shown in Fig. 4a. The nested grid calculation results agree well with the fine grid results while the contamination is in the highly resolved area; however high numerical diffusion appears when the contamination leaves the nested grid. After 24 h of simulation the predictions from the nested grid calculation are more similar to those of the coarse grid calculation than the fine one (Figs. 5–7), showing that the initial advantage of using a nested grid can quickly be lost. The agreement between the adaptive grid solutions (Fig. 3e–h)

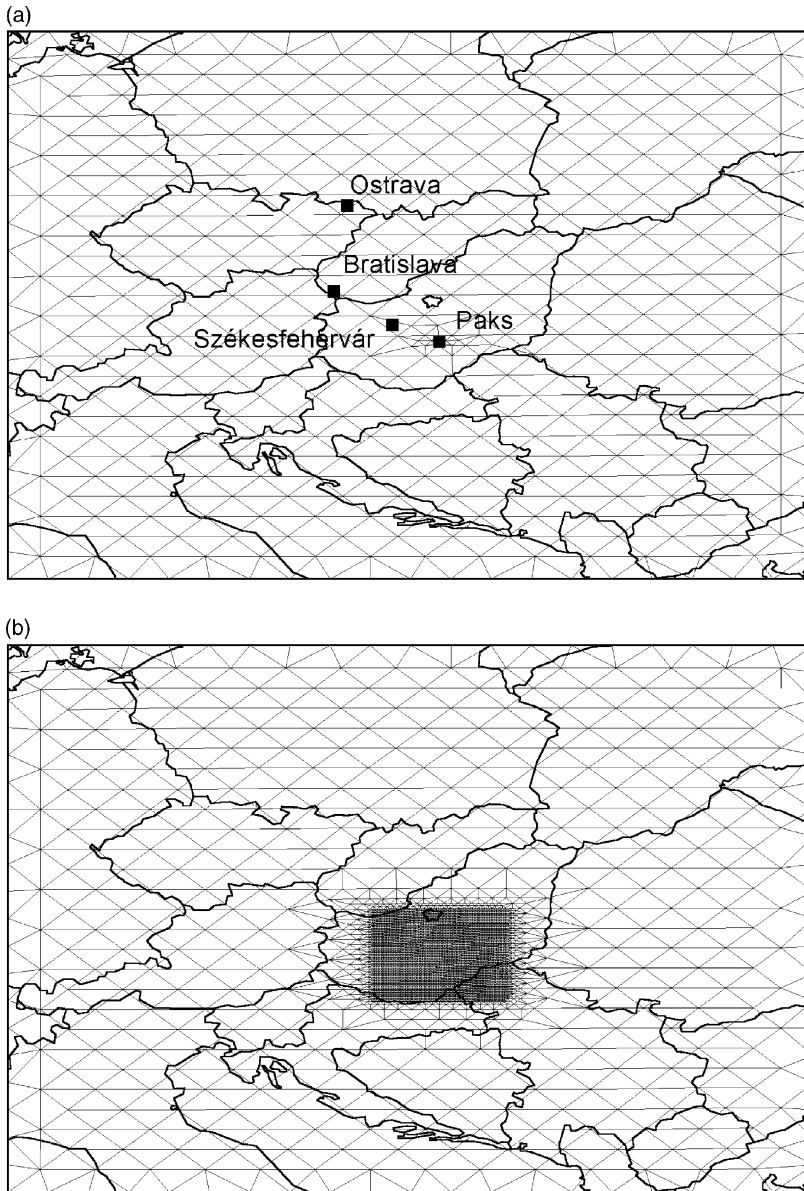


Fig. 2. (a) Initial grid of the adaptive and coarse grid calculations. (b) Nested fine grid within the coarse grid.

and the fine grid results (Figs. 4c, 5c, 6c and 7c) is very good at t_0+12 and t_0+24 h and acceptable at t_0+36 and t_0+48 h simulation times. The shape of the isotope cloud is well predicted with some smearing occurring at the edges. The adaptive grid simulation is significantly closer to the fine grid calculation than both the

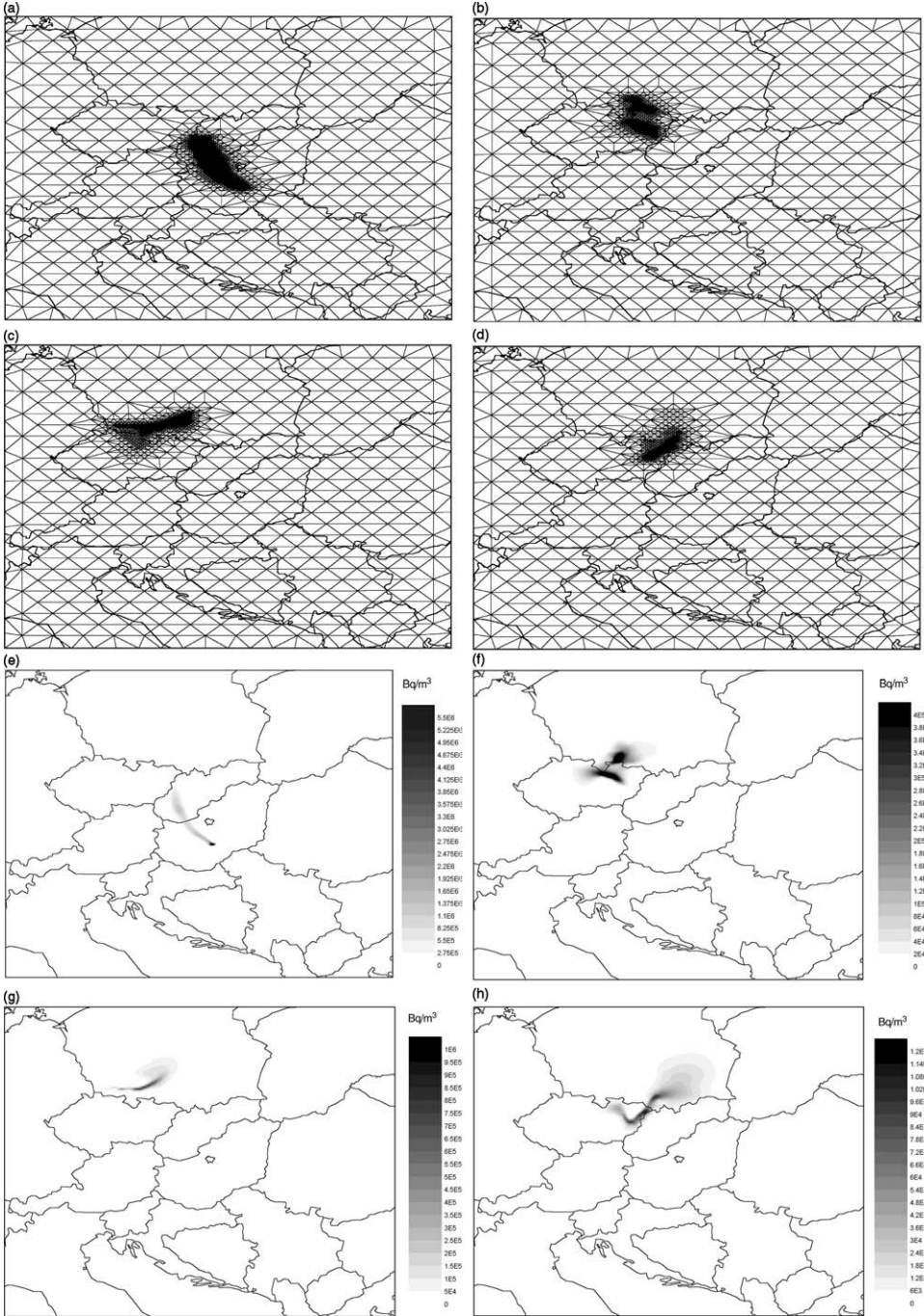


Fig. 3. Change of the surface layer mesh structure and activity of isotope ^{131}I during the adaptive grid calculations. Simulation started from 2 August 1998, at 0.00. (a)–(d) The adapted mesh at t_0+12 , t_0+24 , t_0+36 , t_0+48 h; (e)–(h) activity in the surface layer at t_0+12 , t_0+24 , t_0+36 , t_0+48 h.

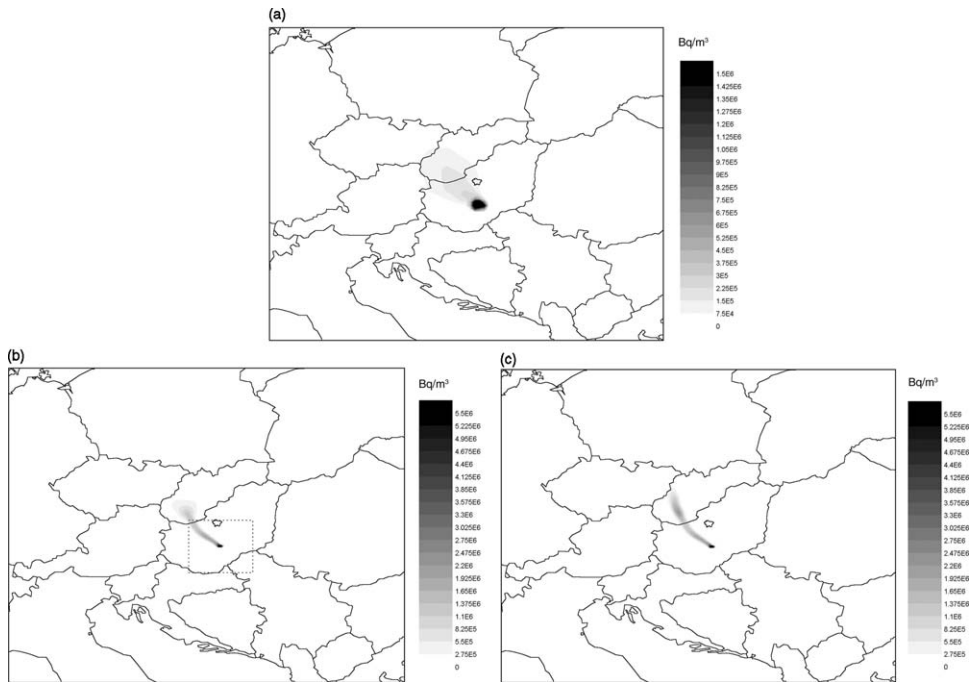


Fig. 4. Surface layer activity of isotope ^{131}I using three different fixed grid size schemes at t_0+12 ((a) coarse grid; (b) nested grid; (c) fine grid). All simulations started from 2 August 1998 at 0.00.

course and nested grid predictions even after 48 h as shown by comparing Figs. 3h and 7.

Nuclear dispersion models have to predict accurately both the maximum level of contamination and the expected arrival time of the contamination peak. The four models presented above can be compared not only by using activity maps at fixed times, but also by plotting the time history of activity at a given location. Three cities, all northwest of Paks were selected: Székesfehérvár (located in Hungary, 101 km from Paks), Bratislava (Slovakia, 247 km), Ostrava (Czech Republic, 415 km). Fig. 8 shows the time dependence of the surface layer activity of ^{131}I in these three cities, calculated by the four gridding schemes. Again, the fine grid calculations were assumed to be the most accurate. At Székesfehérvár, the fine and the nested grid results are identical and the adaptive grid predicted only a slightly higher peak at a slightly earlier arrival time. The coarse grid calculation predicted a much higher double peak arriving much earlier. Bratislava is not affected directly by the plume, as it is well visible from both the fine and the adaptive grid results shown here and in Figs. 3e and 4c. Because of the smearing of the plume due to numerical diffusion however, the coarse and the nested grid models erroneously predict the appearance of the contamination in Bratislava. In a real situation such a prediction may result in the unnecessary evacuation of the population. In Ostrava, the fine

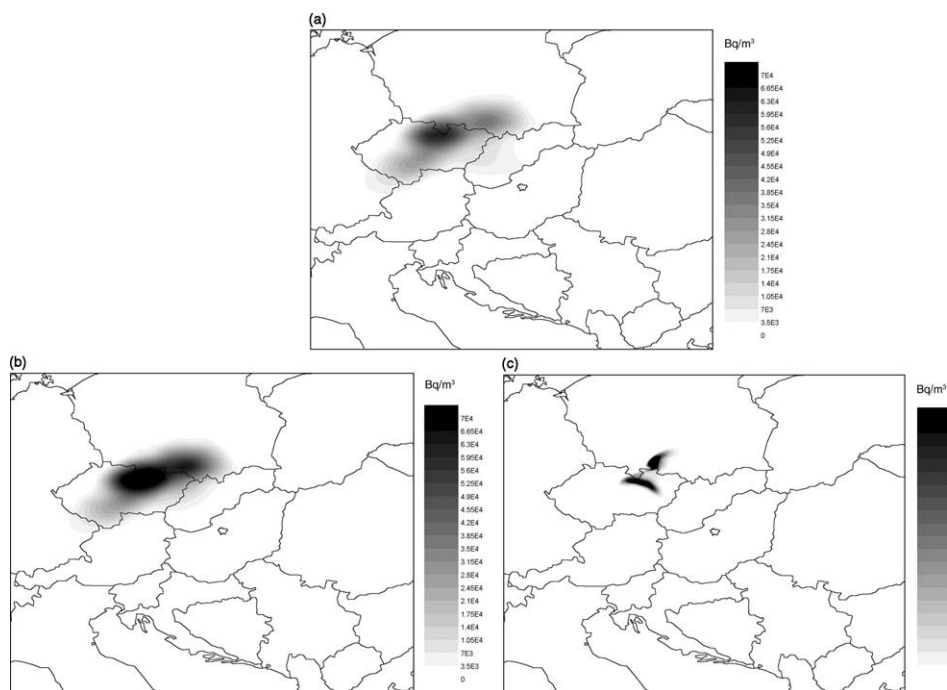


Fig. 5. Surface layer activity of isotope ^{131}I using three different fixed grid size schemes at t_0+24 ((a) coarse grid; (b) nested grid; (c) fine grid). All simulations started from 2 August 1998 at 0.00.

and the adaptive models both predict high contamination at similar arrival times. The nested and the coarse models forecast much lower contamination, which arrives later than predicted by in the fine grid simulations. Based on the latter models, the population may not be evacuated in a dangerous situation. Additionally, the first two models predict the return of the polluted cloud with very good agreement, but such a feature is not present in the course and nested simulation results.

In all cases the fine and adaptive simulation results were in good qualitative agreement, while the coarse and nested grid simulations would have advised wrong measures in the chosen locations. This is also justified by the figures of Table 1, which shows the relative height and time of arrival of the ^{131}I activity calculated from the coarse, adaptive and nested simulations compared to the fine grid simulation results. Outside the nested grid area, the adaptive grid results are always much closer to the fine grid ones. The second column of Table 1 shows that the ratio of time requirements are 1:30:19:532 for the coarse, adaptive, nested and fine grid models, respectively. The adaptive simulation is therefore only slightly more computationally expensive than the nested grid whilst providing a step change in accuracy. Note, that using the time and space dependent adaptive grid is more time consuming than the application of the fixed nested grid due to the use of the

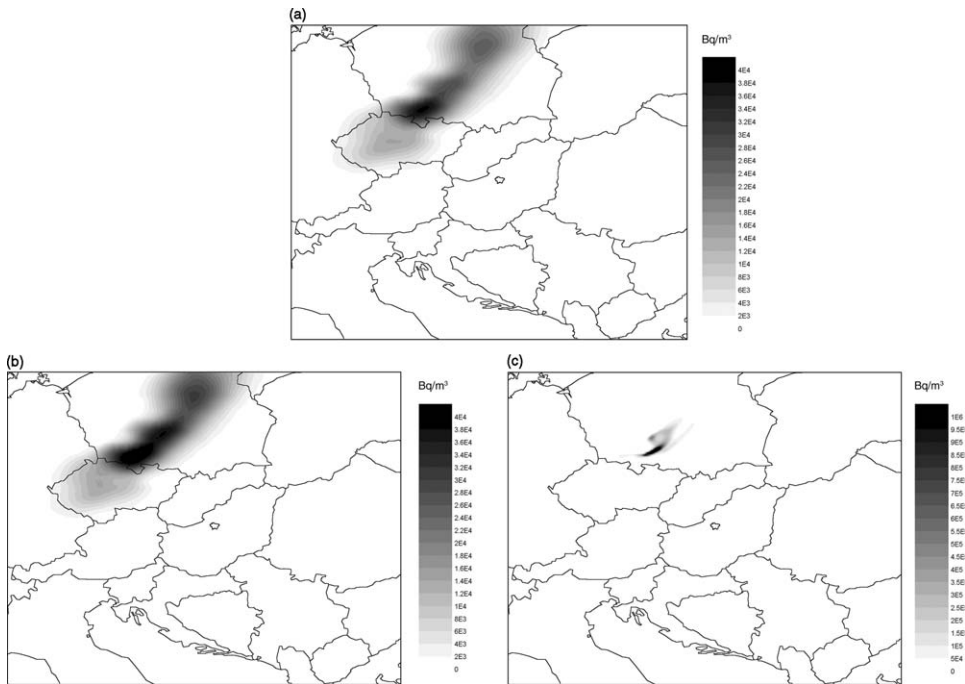


Fig. 6. Surface layer activity of isotope ^{131}I using three different fixed grid size schemes at t_0+36 ((a) coarse grid; (b) nested grid; (c) fine grid). All simulations started from 2 August 1998 at 0.00.

adaptivity algorithm, even though the nested method uses more grid points. There is some overhead therefore in calculating the refinement criteria and interpolating the solution onto the new mesh each time the mesh is updated. However, the fine and the adaptive models provided similar results, but the application of the former required 17.5 times more computer time. The implications could be that given limited computer resources, the adaptive model provides reliable results quickly thus allowing ample time for emergency response. The fine grid model would provide similar results, but possibly too late.

During 2–4 August simulations of the wind-field were almost identical in all vertical layers of the model. However, for some meteorological conditions the direction of the wind may be different at different heights. This condition occurred in Central Europe during 4–6 August 1998. To study the behaviour of the model at such conditions, it was also tested on another assumed nuclear accident starting on 4 August 1998 at time 0.00. All other conditions were identical to the previous case. Fig. 9 shows that at that time there was a slow northeast wind at Paks on the surface and a medium southwest wind above Paks in the upper layer. Accordingly, the contamination drifted southwest within the surface layer (see Figs. 10a,b), and to the northeast in the upper layers. Our multi-layer adaptive grid model predicted that after about 37 h there was a fast exchange of species between the mixing and

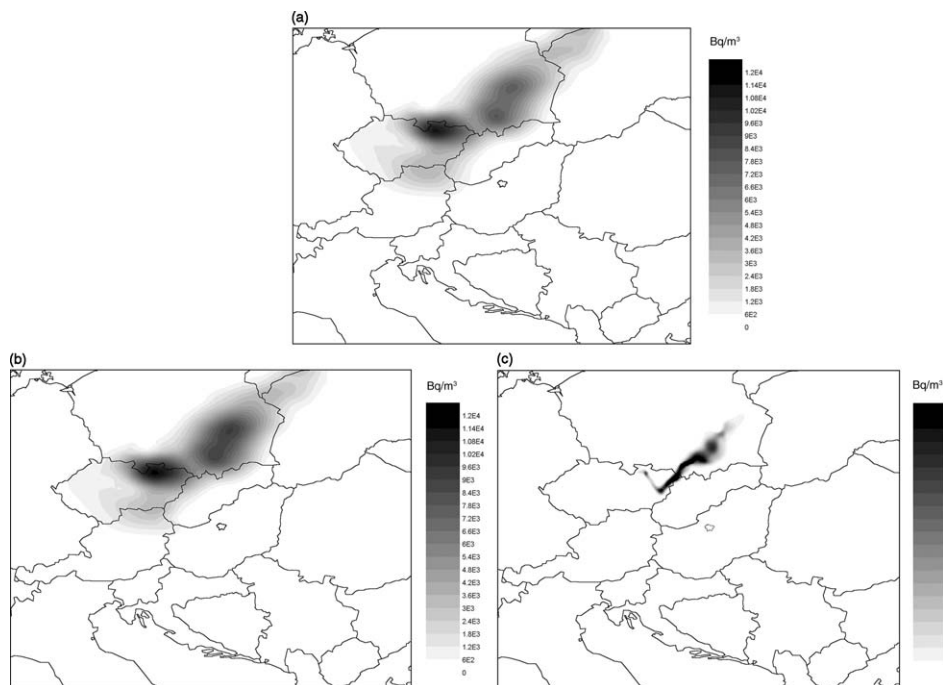


Fig. 7. Surface layer activity of isotope ^{131}I using three different fixed grid size schemes at t_0+48 ((a) coarse grid; (b) nested grid; (c) fine grid). All simulations started from 2 August 1998 at 0.00.

the reservoir and upper layers due to fumigation. Fig. 10c shows at 39 h a large secondary contaminated area appeared northeast from Paks because the upper layer contamination was transported down to the surface by convection. This example emphasises that using high-resolution, detailed meteorological data in several horizontal layers is very important, otherwise even qualitative features such as this one would be ill predicted.

4. Conclusions

An adaptive Eulerian grid model based on triangular unstructured grids describing the dispersion of radionuclides has been developed. The model automatically places a finer resolution grid in regions characterised by high spatial numerical errors and therefore the fine resolution grid automatically follows the spatial concentration gradients resulting from the passage of contaminated air over a given region. This approach allows the achievement of grid resolutions of the order of 6 km without excessive computational effort. The method has been illustrated for sample calculations based on hypothetical nuclear accidents at the Paks NPP in Central Hungary in August 1998. The approach has been shown to be significantly more accurate than a nested grid approach utilising a similar order of

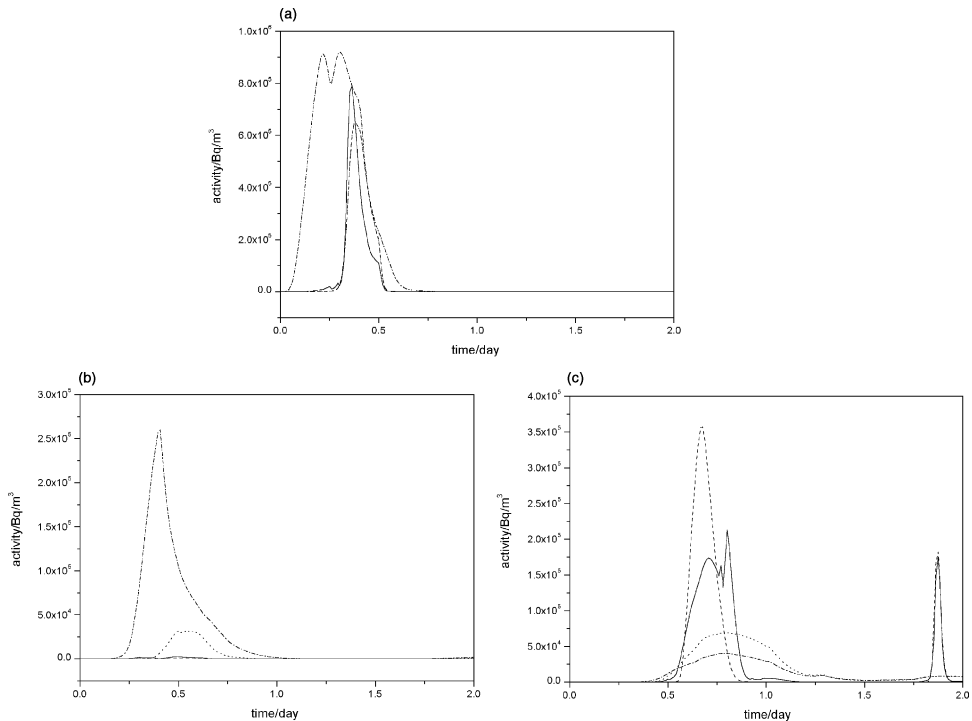


Fig. 8. Time dependence of the surface layer activity of ^{131}I in three cities in the region, calculated using four different gridding schemes. (a) Székesfehérvár (Hungary, 101 km NW from Paks), (b) Bratislava (Slovakia, 247 km NW), (c) Ostrava (Czech Republic, 415 km NW). Solid line, adaptive grid; dashed line, fine grid; dotted line, nested grid; dash-dot line, coarse grid.

computational effort, and to approach the accuracy of a fine grid calculation requiring excessive computer resources. The differences in predicted surface layer activity resulting from various gridding strategies highlights the sensitivity of model accuracy to the numerical methods chosen and grid resolution. The use of inappropriate strategies has been shown to underestimate peak contamination levels in some areas and to erroneously predict the arrival of a contaminated cloud in

Table 1
Comparisons of number of mesh points, CPU times vs. errors for each run

Grid	Relative CPU time	Number of triangles	Relative height and time of arrival of ^{131}I peak at					
			Székesfehérvár		Bratislava		Ostrava	
Coarse	1	844	1.425	-2.88 h	57370	-4.73 h	0.112	2.79 h
Adaptive	30.36	844-3464	1.223	-0.38 h	532	-2.76 h	0.486	0.75 h
Nested	18.86	7368	0.999	0 h	6881	-1.26 h	0.193	2.74 h
Fine	532.22	216064	1	0 h	1	0 h	1	0 h

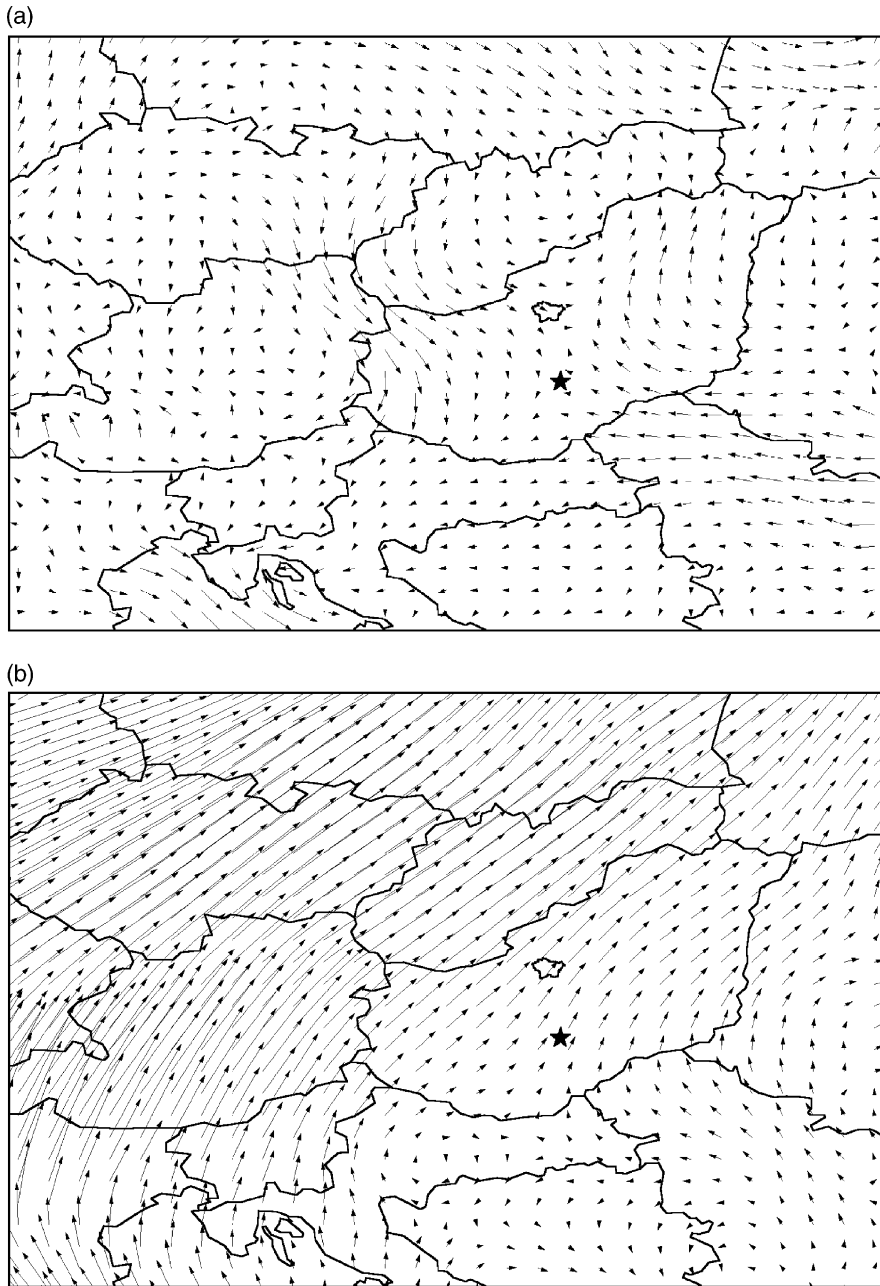


Fig. 9. The wind-field at 0.00 on 4 August (at the start of the second accident scenario) in the surface (a) and upper (b) layers.

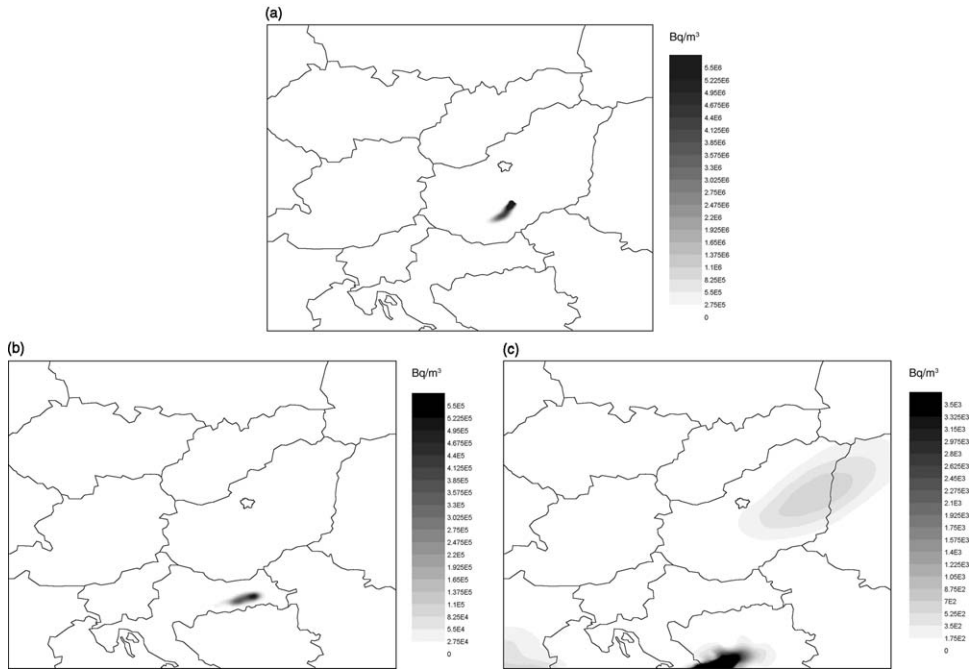


Fig. 10. Simulation of the 4 August accident using adaptive grid. Surface layer activity of isotope ^{131}I at (a) t_0+12 , (b) t_0+24 and (c) t_0+39 h. A secondary polluted area appeared due to contamination from the upper and reservoir layers.

others. Such errors could have important consequences if utilised within emergency response measures. The simulations have also illustrated the impact of meso-scale meteorological structures such as vertical variations in wind-speeds and vertical mixing due to convection on the predicted location of the contaminated cloud at the surface. The results emphasise the importance of coupling a high-resolution dispersion model to a detailed meso-scale meteorological model.

Acknowledgements

The authors acknowledge the helpful discussions with Professor Zoltán Homonnay, and the support of OTKA Grant No. T043770 and UK-Hungarian cooperation Grant No. GB50/98.

References

Baklanov, A., Mahura, A., Jaffe, D., Thaning, L., Bergman, R., Andres, R., 2002. Atmospheric transport patterns and possible consequences for the European North after a nuclear accident. *Journal of Environmental Radioactivity* 60, 23–48.

- Berzins, M., 1994. Temporal error control in the method of lines for convection dominated PDEs. *SIAM Journal of Science Computer* 16, 558–580.
- Berzins, M., Ware, J., 1995. Positive cell-centered finite volume discretization methods for hyperbolic equations on irregular meshes. *Applied Numerical Mathematics* 16, 417–438.
- Berzins, M., Ware, J.M., 1994. Reliable finite volume methods for the Navier Stokes equations. In: Hebekker, F-K., Rannacher, R., Wittum, G. (Eds.), *Notes on Numerical Fluid Mechanics*. Viewg, Wiesbaden, pp. 1–8.
- Berzins, M., Dew, P.M., Furzeland, R.M., 1989. Developing software for time-dependent problems using the method of lines and differential algebraic integrators. *Applied Numerical Mathematics* 5, 375–390.
- Berzins, M., Lawson, J., Ware, J. 1992. Spatial and temporal error control in the adaptive solution of systems of conversation laws. In *Advances in Computer Methods for Partial Differential Equations, IMACS VII*, pp. 60–66.
- Brandt, J., Mikkelsen, T., Thykier-Nielsen, S., Zlatev, Z., 1996. Using a combination of two models in tracer simulations. *Mathematical and Computer Modelling* 23, 99–115.
- Bryall, D.B., Maryon, R.H., 1998. Validation of the UK MET office NAME model against the ETEX data set. *Atmospheric Environment* 32 (24), 4265–4276.
- Clark, M.J., Smith, F.B., 1988. Wet and dry deposition of Chernobyl releases. *Nature* 332, 245–249.
- COST Action 710 1998. Harmonisation of the pre-processing of meteorological data for atmospheric dispersion models. Fisher, B.E.A., Erbrink, J.J., Finardi, S., Jeannet, P., Joffre, S., Morselli, M.G., Pechinger, U., Seibert, P., Thomson, D.J. (Eds.).
- Galmarini, S., Bianconi, R., Bellasio, R., Graziani, G., 2001. Forecasting the consequences of accidental releases of radionuclides in the atmosphere from ensemble dispersion modelling. *Journal of Environmental Radioactivity* 57, 203–219.
- Ghorai, S., Tomlin, A.S., Berzins, M., 2000. Resolution of pollutant concentrations in the boundary layer using a fully 3D adaptive gridding technique. *Atmospheric Environment* 34, 2851–2863.
- Hart, G. 1999. Multi-scale atmospheric dispersion modelling by use of adaptive gridding techniques. PhD. thesis, UK, Leeds.
- Hart, G., Tomlin, A., Smith, J., Berzins, M., 1998. Multi-scale atmospheric dispersion modelling by use of adaptive gridding techniques. *Environmental Monitoring and Assessment* 52, 225–238.
- Horányi, A., Ihász, I., Radnóti, G., 1996. ARPEGE/ALADIN: A numerical Weather prediction model for Central-Europe with the participation of the Hungarian Meteorological Service. *Időjárás* 100, 277–301.
- Joe, B., Simpson, R.B., 1991. Triangular meshes for regions of complicated shape. *International Journal for Numerical Methods in Engineering* 23, 987–997.
- Lagzi, I., Tomlin, A.S., Turányi, T., Haszpra, L., Mészáros, R., Berzins, M., 2001. The simulation of photochemical smog episodes in Hungary and Central Europe using adaptive gridding models. *Lecture Notes in Computer Science* 2074, 67–77.
- Lagzi, I., Tomlin, A.S., Turányi, T., Haszpra, L., Mészáros, R., Berzins, M., 2002. Modelling photochemical air pollution in Hungary using an adaptive grid model. In: Sportisse, S. (Ed.), *Air Pollution Modelling and Simulation*. Springer, Berlin, pp. 264–273.
- Langner, J., Robertson, L., Persson, C., Ullersig, A., 1998. Validation of the operational emergency response model at the Swedish meteorological and hydrological institute using data from ETEX and the Chernobyl accident. *Atmospheric Environment* 32, 4325–4333.
- Nasstrom, J.S., Pace, J.C., 1998. Evaluation of the effect of meteorological data resolution on Lagrangian particle dispersion simulations using the ETEX experiment. *Atmospheric Environment* 32 (24), 4187–4194.
- Pudykiewicz, J., 1989. Simulation of the Chernobyl dispersion with a-D hemispheric tracer model. *Tellus* 41B, 391–412.
- Pudykiewicz, J., 1991. Environmental prediction system: Design, implementation aspects and operational experience with application to accidental release. In: van Dop, H., Steyn, D.G. (Eds.), *Air Pollution Modelling and its Application VIII. NATO Challenge of Modern Society*, 15. Plenum Press, New York, pp. 561–590.

- Saltbones, J., Foss, A., Bartnicki, J., 1998. Norwegian Meteorological Institute's real-time dispersion model SNAP (Severe Nuclear Accident Program); Runs for ETEX and ATMES II experiments with different meteorological. *Atmospheric Environment* 32 (24), 4277–4283.
- Sørensen, J.H., 1998. Sensitivity of the DERMA Long-range Gaussian dispersion model to meteorological input and diffusion parameters. *Atmospheric Environment* 32 (24), 4195–4206.
- Tomlin, A., Berzins, M., Ware, J., Smith, J., Pilling, M.J., 1997. On the use adaptive gridding methods for modelling chemical transport from multi-scale sources. *Atmospheric Environment* 31, 2945–2959.
- Tomlin, A.S., Ghorai, S., Hart, G., Berzins, M., 2000. 3-D Multi-scale air pollution modelling using adaptive unstructured meshes. *Environmental Modelling and Software*, 15, 681–692.
- Van Dop, H., Addis, R., Fraser, G., Girardi, F., Graziani, G., Inoue, Y., Kelly, N., Klug, W., Kulmala, A., Nodop, K., Pretel, J., 1998. ETEX: A European Tracer Experiment; Observations, dispersion modelling and emergency response. *Atmospheric Environment* 32, 4089–4094.
- Van Loon, M. 1996. Numerical methods in smog prediction. PhD. thesis, GWI Amsterdam.
- Verver, G., De Leeuw, M., 1992. An operational puff dispersion model. *Atmospheric Environment* 26A, 3179–3193.
- Ware, J., Berzins, M., 1995. Adaptive finite volume methods for time-dependent PDEs. In: Babuska, I., et al.(Eds.), *Modeling Mesh Generation and Adaptive Numerical Methods for PDEs*. Springer, Berlin, pp. 417–430.
- Wendum, D., 1998. Three long-range transport models compared to the ETEX experiment: a performance study. *Atmospheric Environment* 32, 4297–4305.
- Whicker, F.W., Shaw, G., Voigt, G., Holm, E., 1999. Radioactive contamination: state of the science and its application to predictive models. *Environmental Pollution* 100, 133–149.